

Ryerson University  
Faculty of Engineering and Architectural Science  
Department of Aerospace Engineering

INVESTIGATION OF FALCON DIVE  
AND DEVELOPING KINEMATIC APPROACH  
AADIL MULLA

AER 870  
Aerospace Engineering Thesis  
Faculty Advisor – Dr. Goetz Bramesfeld  
16/04/2021

## ACKNOWLEDGEMENT

The Author would like to express gratitude to Dr. Goetz Bramesfeld, for his consultation and support throughout this project. The feedback provided was invaluable in achieving the results.

The Author would also like to thank Ryerson University and the Department of Aerospace Engineering for providing this opportunity to work on an Undergraduate Thesis project. Furthermore, the Author would like to thank friends and family for their continuous support throughout the project.

## ABSTRACT

This study investigates the aerodynamic methods already implemented in studying a peregrine falcon dive. The paper presents a literature review of aerodynamic methods, starting from mathematical models aimed at predicting falcon dive using minimum drag theory. This is followed by experimental methods that developed the flight path trajectory using high-tech cameras. Additionally, the paper presents numerical analysis of the falcon body model using computational fluid dynamics and particle image velocimetry in order to assess and derive aerodynamic coefficients. Based on the research, a kinematic model for the problem was developed, and the reason for failure were highlighted.

# CONTENTS

1. INTRODUCTION.....	1
2. LITERATURE REVIEW .....	2
3. KINEMATIC DIVE MODEL .....	13
4. ATTEMPTED MODEL AND DISCUSSION .....	15
5. CONCLUSION .....	16
6. REFERENCES .....	17
APPENDIX.....	18
Developing Flight Path Angle Equation.....	18
Developing Drag Polar Equation .....	18
Plotting Graphs .....	18

## LIST OF FIGURES

Figure 1: Typical Shape of Peregrine Falcon in fast steep dive. ....	1
Figure 2: Detailed pictures depicting falcon body shapes throughout dive. ....	2
Figure 3: Flight path of a Peregrine Falcon in stoop with corresponding phases. ....	4
Figure 4: Force vectors during equilibrium .....	5
Figure 5: Arc followed during dive pull out. ....	7
Figure 6: A life size model of falcon. ....	8
Figure 7: Force balance wind tunnel set-up. ....	9
Figure 8: Open Cupped (Left) and Cupped Shape model (Right) .....	11
Figure 9: Surface streamline pattern showing flow topology over falcon .....	12
Figure 10: Falcon dive coordinate system .....	13
Figure 11: Phases of Falcon Dive.....	14
Figure 12: Forces acting on falcon when in non-equilibrium phase.....	15

## LIST OF SYMBOLS

$a_n$  – Normal Acceleration

$a_t$  – Tangential Acceleration

AR – Wing Aspect ratio

$\alpha$  – Angle of attack

b – Wingspan

$b_0$  – Wingspan for minimum drag

$C_L$  – Coefficient of Lift

$C_D$  – Coefficient of Drag

$C_{LT}$  – Theoretical Lift Coefficient for delta wing

$C_{LP}$  – Potential flow lift coefficient

$C_{LV}$  – Vortex flow lift coefficient

$D_{pr}$  – Profile Drag

$D_{par}$  – Parasitic Drag

$D_{in}$  – Induced Drag

$D_{min}$  – Minimum Drag

D – Drag

$f$  – Mathematical Function

$F_t$  – Tangential Force

$F_s$  – Transversal force

$F_L$  – Longitudinal force

F – Resultant Force

g – Acceleration due to gravity

$K_p$  - Potential flow constant

$K_v$  – Vortex flow constant

L – Lift

$L_1$  - Maximum lift

m – mass of the body/object

$q$  – Dynamic Pressure

$Re$  – Reynolds Number

$\rho$  – Density

$S_w$  – Upper reference area of falcon

$S_b$  – Maximum cross-sectional area of the body

$s$  – distance

$\theta_0$  – Initial glide path angle

$\pi$  – ratio of circumference to diameter of a circle

$\dot{\theta}$  – Angular velocity

$\theta$  – Glide path angle

$\mu$  – Dynamic Viscosity of air

$V$  – Instantaneous velocity

$V_E$  – Equilibrium glide speed

$W$  – magnitude of body weight

$x, y$  – Spatial coordinates

$\Delta y$  – altitude drop

## 1. INTRODUCTION

Many birds of prey attack using high-speed dives in order to hunt while being airborne. One of them is Peregrine Falcon; they are large, quick predatory birds with strong, sharp, yellow talons that enable them to hunt other birds, even during flight. [1] Before diving the falcon usually gains speed and accelerates by flapping its wings, and once it begins the dive, the wings fold and alter throughout the flight to control the aerodynamics and flight characteristics. [2] During the initial phase, the falcon accelerates by folding its wing closer to the body, wherein, it takes up the shape of a tear drop in order to reduce drag. Soon after, the falcon slowly opens up its wing to take the form a cupped shape structure around its body. This is followed by opening wings slowly to increase drag and decelerate thus allowing for flight path correction. Lastly, after catching its prey, the falcon slowly pulls out of the dive by spreading its wings away from body and thus producing lift. [2]

The speeds reached during the dive are limited by aerodynamic properties of the bird such as flight path angle, acceleration due to gravity, distance to the ground, and time available for flight. It might occur to some, as to why the falcon needs to dive to hunt; this is because, during horizontal flight, it reaches velocities up to  $150 \text{ km h}^{-1}$  only. [2] Which often is not sufficient enough to capture the target. The research will aim at producing a theoretical model describing flight kinematics, however, it must be noted that in nature, falcons do not necessarily follow the same pattern.

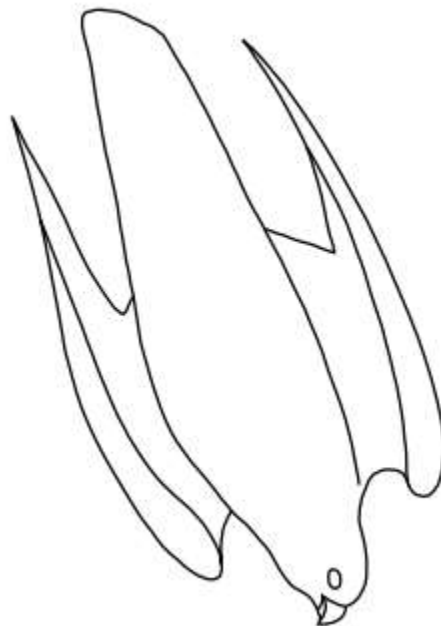


*Figure 1: Typical Shape of Peregrine Falcon in fast steep dive. [3]*

## 2. LITERATURE REVIEW

The flight of the peregrine falcon is a very short, rare, unpredictable event taking place in nature. It is difficult to analyse and capture the dive in its true form. Therefore, attempts have been made to capture falcon dive using trained falcon and mimic the dive in its original form. [2] This research uses experiment performed by Ponitz et al. that documents the dive of a trained falcon from a dam. [2] The experiment was conducted using high speed cameras that recorded the flight path characteristics and position of the falcon at different times.

Accordingly, the flight was divided into six phases, and they are as follows [2]:

- a. Acceleration/diving phases (0 - 1.1s)
- b. Transient phase with roughly constant speed (1.1 - 1.3s)
- c. Deceleration and flight correction phase (1.3 - 2.3s)
- d. Pull out phase (2.3 - 3.5s)
- e. Landing phase with constant speed (3.5 - 5.0s)
- f. Landing phase with deceleration and touchdown (5.0 - 6.8s)

However, only phases a-c will be focused on in the scope of this paper. The shapes and phases are described in detail below.

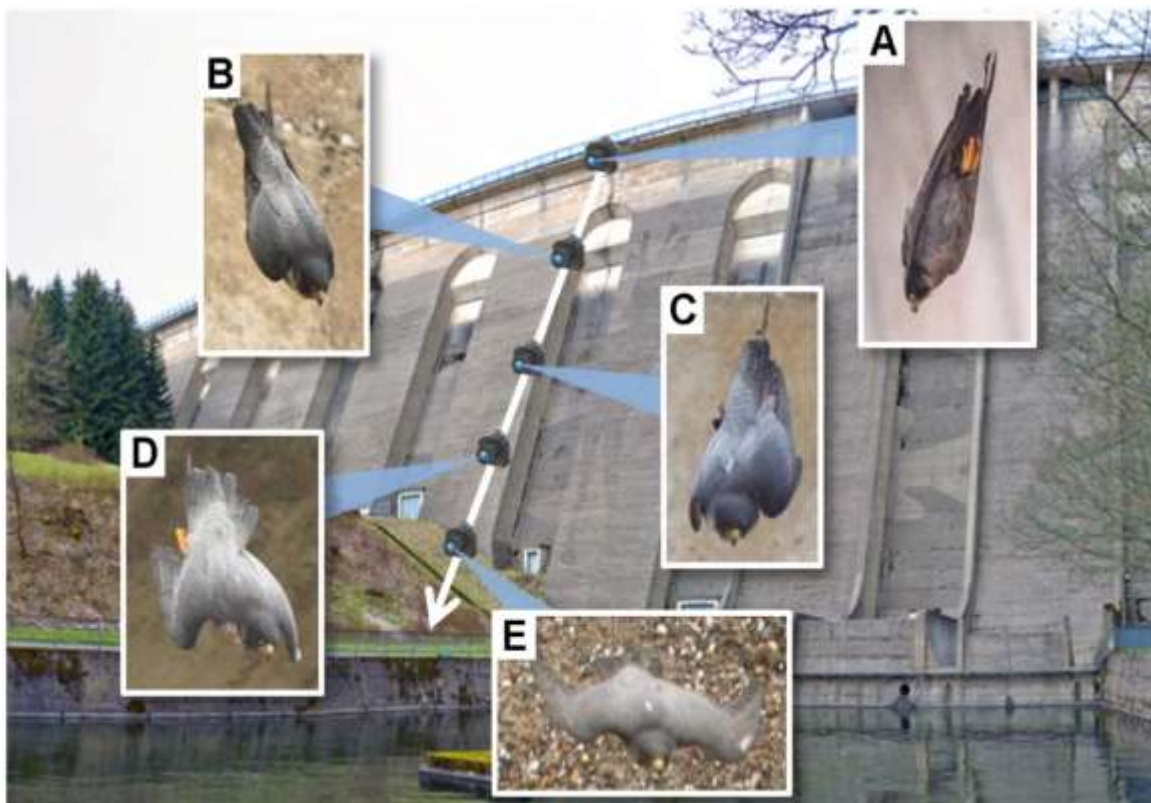


Figure 2: Detailed pictures depicting falcon body shapes throughout dive. [2]

## TEAR DROP SHAPE

Initially the falcon accelerates; in this phase it takes up a tear drop shape. It does so by completely retracting the wings into the body and keeping the tail completely furled. [4] Due to complete retraction of wings, it can be said that the bird has little to no control and can be considered as an unguided projectile optimizing for maximum speed. [4] If a falcon intends to maximize velocity during hunt, the falcon does so during this configuration.

## CUPPEDSHAPE

Gradually, the bird will adjust in a way, that it starts pushing the leading edge of the wing laterally away from the body, while the trailing edge is still attached to the tail. [4] When the bird takes up cupped-shape configuration (also referred to as C-shaped), the bird creates a ‘cup’ of air between its wing and body, and it is also during this configuration that the bird adjusts its trajectory. [4] Through the C-shape configuration, the falcon body produces a cavity between the wing and body. [5] Opening up the wings further to maximize the cavity results in a lesser flow acceleration and hence increases the form drag. [5] The vortices produced during this configuration enable the falcon to control pitch and roll moment and hence allowing the falcon to have higher manoeuvrability. [5]

## M-SHAPE

The last configuration adopted in which the bird is pulling out of a dive is M-shape configuration. During this phase, the arm opens up further into the horizontal plane and the wings are aligned in a way that the bird appears to be in an M-shaped planform when seen from above. [6] In this phase, the trailing edge of wing detaches from the body, such that there is a forward sweep in the in-board section and aft sweep in the outboard section of the wing. [4] As the falcon goes deep into pull out maneuver, there is a reduction in sweep angle in the outboard section of the wing. [4] Moreover, the forward sweep directs the span wise flow in board, which leads to flow reattachment. [4] This flow reattachment improves manoeuvrability. [5] It is also in this phase that the falcon adjusts its trajectory or corrects its attitude rapidly, thereby increasing the chances of striking the prey. [4]

It is to be noted that there is rather a smooth transition from one phase to another, which is often reversed in nature. [4] From the literature above, it can be asserted that Cupped-shape and M-shape configuration of the falcon body are very crucial during stoop and pull-out phases of the dive. Without a doubt, the success of attacks can be largely associated with the manoeuvrability during these phases. [6] This paper aims at performing literature review in order to provide better intuition on the kinematics of falcon dive trajectory. In the past, various attempts have been made to study the falcon dive, from producing mathematical models to performing CFD analysis on different phases of the model during the dive. A deeper study of these methods will show whether there exists any particular method in its entirety that can be used to predict falcon dive characteristics.

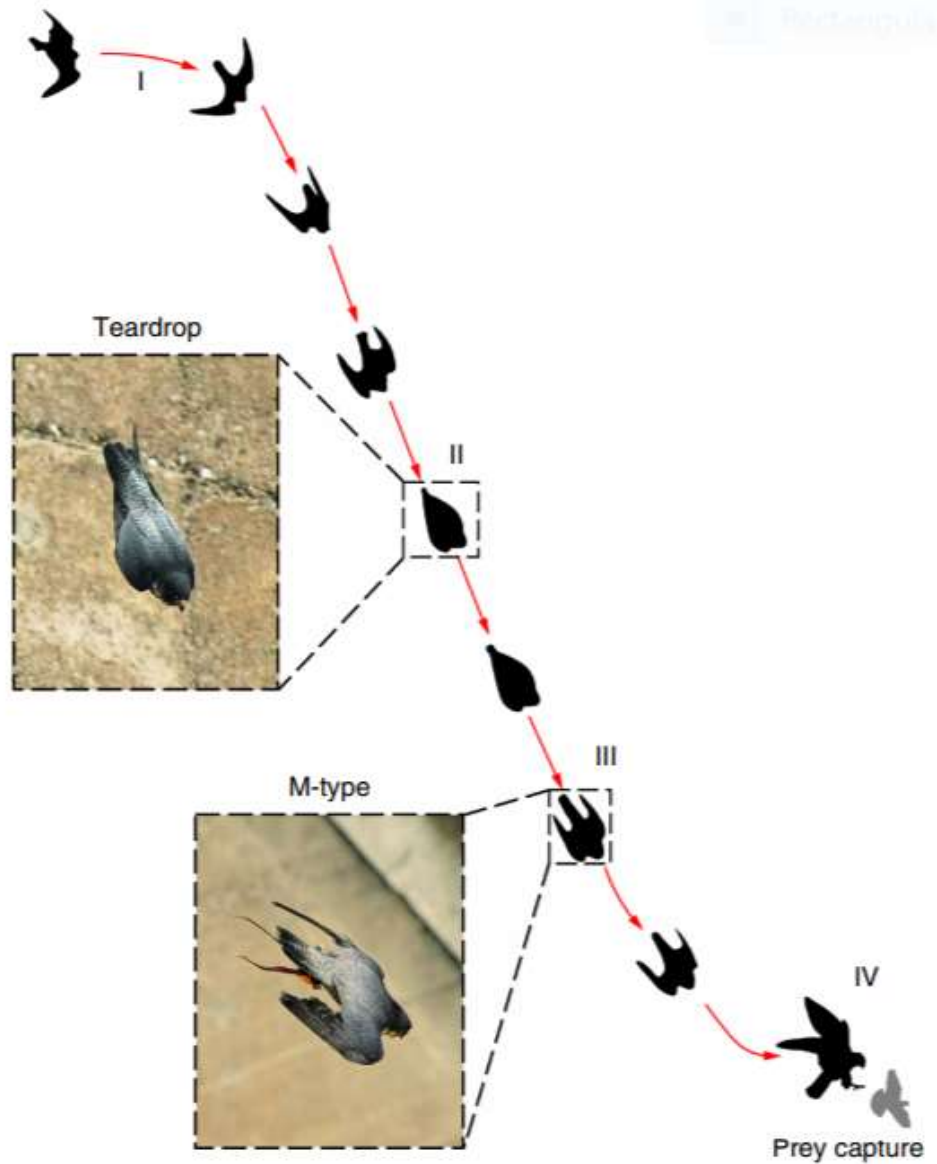


Figure 3: Flight path of a Peregrine Falcon in stoop with corresponding phases. [6]

In Aerodynamics, there are three main ways of predicting or analysing the aerodynamic performance of a body, namely, analytical model, numerical simulations, and experimental tests. An analytical or mathematical model is used to represent a specific problem, and in general it is derived from simple physical values. On the contrary, numerical simulations are widely used to solve complex problems, since it is cost effective but is often very time consuming. Nonetheless, the outcome of both the former methods can be confirmed using experimental methods, which are more robust. The literature review will aim to study different methods and models that have already been performed in order to predict falcon flight dive.

### ***Mathematical approach to recreate falcon dive.***

Several mathematical models are available for representing a falcon dive, however, only two main models will be presented, both of which have been developed from the models before them. In Tucker's mathematical model from 1987, the author presented and worked only on equilibrium gliding, that is, it considered the non-accelerated dive phase only. [7] Nonetheless, Tucker's model of 1998 accounted for acceleration during the dive or during the subsequent pull out. [3] The experiment, performed by the author, traced out a position vector  $P$  along the falcon's glide path angle  $\theta$  and change in flight path angle with respect to horizontal axis. [3] The position vector was then differentiated to obtain the velocity vector describing the falcon's flight path. [3] A summary of both phases of the flight path developed above, i.e., equilibrium and non-equilibrium phases, have been presented below.

#### **a. Equilibrium Gliding:**

According to Tucker's model of 1987, for a falcon to have maximum performance during equilibrium flight, it must alter its shape to ensure that the wing produces lift equal to  $W\cos\theta$ , where  $W$  denotes weight, as shown in Fig. 4. The body must have a minimum drag at equilibrium speed,  $V_E$ . [7]

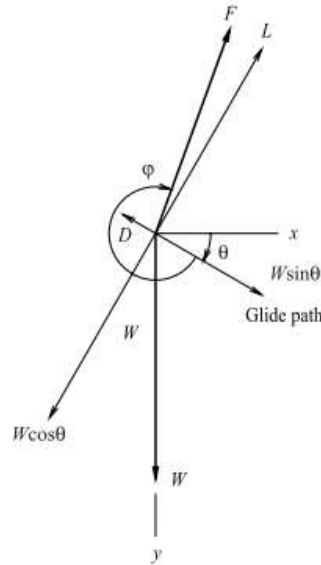


Figure 4: Force vectors during equilibrium [3]

The dynamic pressure can be obtained using the velocity obtained after the position vector differentiation, and the density  $\rho$ , by using Eq. 1. [3]

$$q = 0.5\rho V^2 \quad (1)$$

Additionally, the Reynolds number,  $Re$ , influences drag coefficients, which in turn impacts the overall drag, and it can be obtained by using Eq. 2. [3]

$$Re = \rho dV/\mu \quad (2)$$

Where,  $d$  is length of the falcon model, and  $\mu$  being the dynamic viscosity of air. From Fig. 4, Eq. 3. can be derived to obtain lift,  $L$ , of the falcon. Further, to obtain the coefficient of lift,  $C_L$ , Eq. 4 was used, where  $S_w$  is the upper surface area of falcon. [3]

$$L = W \cos \theta \quad (3)$$

$$C_L = \frac{L}{q S_w} \quad (4)$$

The total drag is the sum of the induced drag,  $D_i$ , profile drag,  $D_{pr}$ , and the parasitic drag,  $D_{par}$ . Induced drag is created as a result of lift production, and Eq. 5 was used to obtain the induced drag, where  $b$  is the wingspan. [3]

$$D_i = \frac{1.1L^2}{\pi q b^2} \quad (5)$$

Similarly, the profile drag was obtained using Eq. 6, wherein the profile drag coefficient  $C_{D_{pr}}$  was obtained using the relation expressed by Eq 7. [3]

$$D_{pr} = q S_w C_{D_{pr}} \quad (6)$$

$$C_{D_{pr}} = 0.0512 - 0.084 C_L + 0.0792 C_L^2 \quad (7)$$

Finally, the parasitic drag was obtained using Eq. 8, and it was assumed that the coefficient of parasitic drag,  $C_{D_{par}}$ , remained constant for the falcon of constant mass,  $S_b$  is maximum cross-sectional area of the body [3]

$$D_{par} = q S_b C_{D_{par}} \quad (8)$$

Here, an ideal falcon was assumed which did not change its tail orientation much throughout the diving phase. [3] However, in reality, this is not true, since the parasitic drag coefficient varies with changes in the falcon's body shape, and this can be confirmed by cross checking the pictures provided in Ponitz et al. Moreover,  $C_{D_{par}}$  is very susceptible to changes in Reynolds number, that is, it declines with increasing  $Re$  and it is highly likely that it does so in real falcons as well. [3] After obtaining all the drags, the total drag was obtained by summing up Eq. 5, 6 and 8 for a given speed. [3] The mathematical model is built considering that the maximum performance speed occurs at minimum drag,  $D_{min}$ . Therefore, to find the maximum performance curves for the ideal falcon, the partial derivative was set to 0, and then the  $D_{min}$  and the wingspan for minimum drag,  $b_0$ , were derived as a function of velocity, as shown in Eq. 9 and 10.

$$D_{min} = f_1(V) \quad (9)$$

$$b_0 = f_2(V) \quad (10)$$

The model above can be solved iteratively using a system of equations to obtain the plot of velocity for maximum performance during equilibrium phase of diving.

**b. Non-Equilibrium Gliding:**

As per Tucker’s model of 1998, non-equilibrium diving phase is when the falcon accelerates along a straight glide path at an inclined angle  $\theta$ . [3] For this analysis, it was assumed that throughout the acceleration phase, the falcon adjusted its wingspan to minimize  $C_{D_{par}}$ . [3] The acceleration along the glide path angle was expressed using Eq. 11, wherein, Eq. 9 was used to depict drag during accelerated flight. [3]

$$\frac{dV}{dt} = g \sin\theta - f_1(V)/m \tag{11}$$

Since the glide path angle is considered to be constant during acceleration, the solution to Eq. 11 can be found out numerically to obtain velocity as a function of time, as shown in Eq. 12. [3]

$$V = f_3(t) \tag{12}$$

Likewise,  $b_0$  changes with velocity, and this was found out by numerically solving Eq. 10 and 12.

$$b_0 = f_4(V) \tag{13}$$

The distance,  $s$ , travelled by the falcon was obtained using Eq. 14, where  $y$  represents the falcon’s altitude loss.

$$y = s \sin\theta \tag{14}$$

The functions  $f_1 - f_4$  are mass-related characteristics of the ideal falcon; more information on them can be found in Tucker VA 1998. [3] These functions were solved using system of equations to obtain the velocity reached with minimum drag configuration for acceleration at constant flight path angle.

**c. Pull out maneuver:**

In case of a non-equilibrium pull out from a dive, it was assumed that the speed remained constant along the circular arc until the glide path angle was aligned with the horizontal. [3]

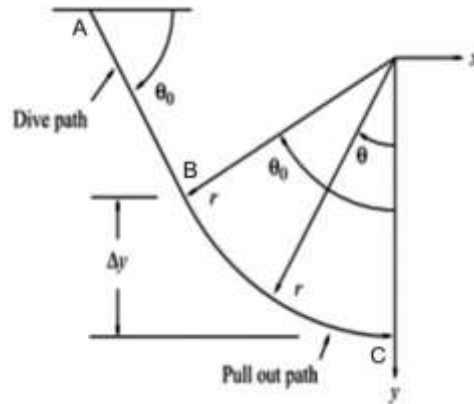


Figure 5: Arc followed during dive pull out. [3]

Accordingly, when the falcon followed a circular arc path of radius,  $r$ , it was assumed that the constant centripetal force component was generated throughout the dive. [3] From Fig. 5, at point C, the weight,  $W$ , acts downwards and  $L_1$  is the maximum lift at that point. This is depicted by Eq. 15 as follows.

$$L_1 - W = \frac{mV^2}{r} \quad (15)$$

The loss in altitude,  $\Delta y$ , depends on the total change in  $\theta_0$  and can be expressed using Eq. 16. [3]

$$\Delta y = r(1 - \cos\theta_0) \quad (16)$$

Finally, the total loss in altitude can be obtained by combination of Eq. 15 and 16. [3]

$$\Delta y = \frac{mV^2(1 - \cos\theta_0)}{L_1 - W} \quad (17)$$

The model failed to consider the lift generation during the transient phase (cupped and open cupped phase), since not enough was known to allow for the accurate calculation of the drag experienced by the falcon, wherein most of the lift is due to vortex generation and flow acceleration. [6] The model failed to account for additional lift during both, the transient phase, and the teardrop phase.

### ***Experimental approach and wind tunnel investigations***

In the experiment performed by Ponitz et al. [2], the author experimented with a falcon trained to dive from a 60 m high dam wall. The research used stereo camera calibrations and a triangulation method to reconstruct a three-dimensional flight path trajectory. [2] The experimental photographs were used to generate the corresponding contours using a stuffed body of a female peregrine falcon, and by manually modifying its wings, a 3D scan of the falcon model for maximum velocity was able to be created, as shown in Fig 6. Finally, this 3D scanned model was used to create a 1:1 scaled polyvinyl chloride model using CNC fabrication process, which was then used in the wind tunnel investigation.

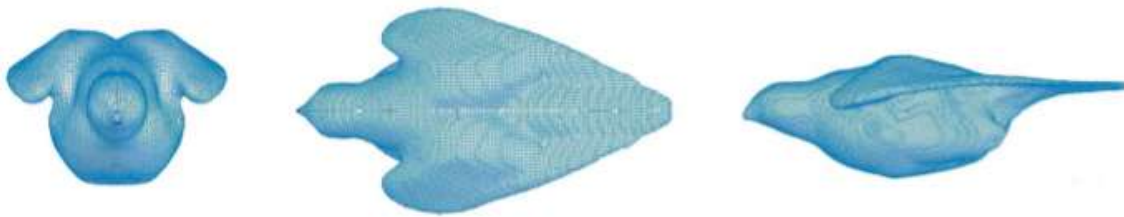


Figure 6: A life size model of falcon. [2]

The 3D fabricated model was mounted on the sting of a force-balance device and was placed in the wind tunnel. [2] This setup consisted of load cells that acquired longitudinal force,  $F_L$ , and transversal force,  $F_S$ . The values of transverse and longitudinal forces obtained through load cells at different angles of attack,  $\alpha$ , are used to obtain lift,  $L$ , and drag,  $D$ , using Eq. (18) and Eq. (19). [2]

$$L = F_s \cdot \cos\alpha - F_L \cdot \sin\alpha \quad (18)$$

$$D = F_s \cdot \sin\alpha - F_L \cdot \cos\alpha \quad (19)$$

The force balance systems depicting Eq. 18 and 19, are represented in Fig. 7. The lift and drag forces are then reduced to their corresponding coefficients using Eq. 20 and Eq. 21. Here,  $C_L$  and  $C_D$  are the coefficients of lift and drag respectively,  $q$  is the dynamic pressure, and the area of the falcon's upper surface is given by  $A_{ref\ top} = 0.041\ m^2$ . [2]

$$C_L = \frac{L}{q \cdot A} = \frac{2L}{\rho v^2 A} \quad (20)$$

$$C_D = \frac{D}{q \cdot A} = \frac{2D}{\rho v^2 A} \quad (21)$$

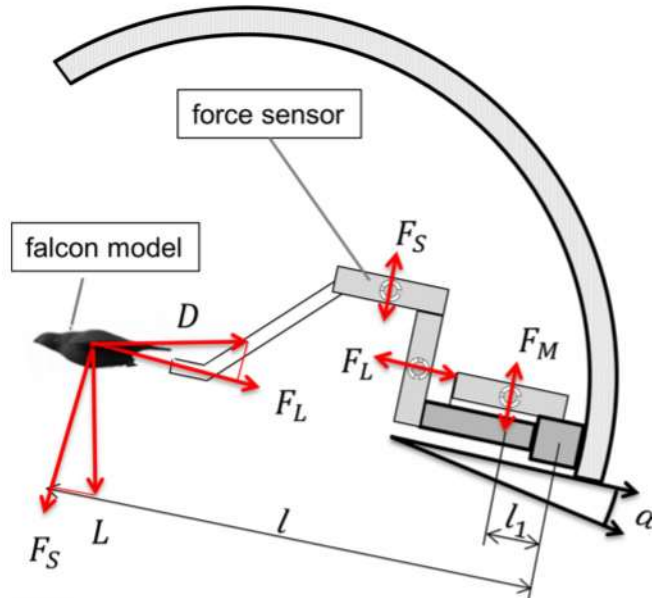


Figure 7: Force balance wind tunnel set-up. [2]

One of the feasible methods implemented by Ponitz et al. was to obtain the position vectors of the falcon using 3D trajectory, which can then be used to obtain velocity vectors. [2] However, this resulted in position inaccuracies, which caused deviation errors, and therefore, moving spline interpolation was used to obtain the flight velocity at different positions in space at their respective times. [2] Nonetheless, it must be noted that the values of velocity and acceleration obtained through this method are not very reliable. [8] Spline interpolation, like any other interpolation process, has a high margin of distortion due to noise, especially when the derivatives are estimated by differentiating the interpolating spline. [8] The work performed above only provided insights on the aerodynamics of the falcon body during equilibrium phase. Furthermore, the research gap of how lift was produced during cupped and open cupped phases still remained unbridged.

The method was further worked on by Selim et al. wherein, the author aimed at exploring the aerodynamics of M-shape configuration towards the end of pull out. [4] Exploring the M-shape configuration of the falcon dive provided insights on maximum forces the bird would need to withstand at superior flight speeds. [4] Further analysis showed that the falcon adopted M-shape configuration to vary the amount of lift production in order to minimize the load factor, thereby, enabling a smooth and steady pullout from the dive. [4] Conversely, this can also be attributed to the fact that the falcon gets into the M-shape configuration to ‘kill’ lift such that it does not exceed the maximum tolerable bending torque that it might face. [9]

In addition, the wing shape during the M-shape configuration depicted more of a delta wing. For a delta wing in subsonic flow, the theoretical lift coefficient,  $C_{LT}$ , generated was derived from Polhamus. [4][10] Theoretically, the lift is the sum of the potential flow lift,  $C_{LP}$ , and vortex flow,  $C_{LV}$ . [10] This is depicted as follows,

$$C_{LT} = C_{LP} + C_{LV} \quad (22)$$

$$C_{LP} = K_P \sin \alpha \cdot \cos^2 \alpha \quad (23)$$

$$C_{LV} = K_V \sin^2 \alpha \cdot \cos \alpha \quad (24)$$

In Eq. 23 and 24,  $K_P$  and  $K_V$  are potential flow and vortex flow constants respectively, for a given aspect ratio wing. [4] For instance, when aspect ratio,  $AR = 1$ , the resulting potential and vortex flow coefficients are the following:  $K_P = 1.2$ , and  $K_V = \pi$ . [4][10] Nonetheless, the outcomes of work done by Selim et al. only provided theoretical models and their confirmations through numerical simulations. However, it lacked any robust validation through experimental testing for M-shape configuration.

### ***Numerical simulations using computational fluid dynamics:***

As evident from earlier work done, the aerodynamics of cupped, open-cupped, and M-shape phases were still not fully understood. Therefore, it was necessary to conduct further research to fully understand it. As per Ponitz et al., the cupped wing configuration is when wings are downward tilted and aimed at adopting a marginal deceleration to adjust its trajectory. [11] On the contrary, the open-cupped wing configuration is an intermediate configuration between the cupped shape and tear drop shape, mainly concerned with control and maneuverability. [11] In order to better understand aerodynamics of these configurations, computational fluid dynamics was performed with the help of ICEM CFD, and Open FOAM. [11]

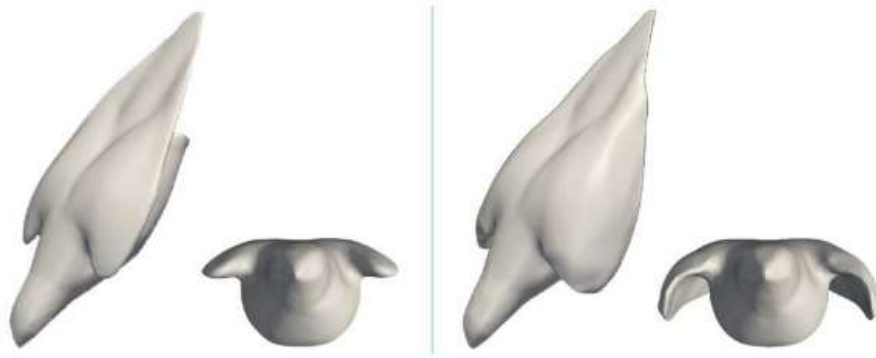


Figure 8: Open Cupped (Left) and Cupped Shape model (Right) [12]

The numerical simulation enabled the calculation of integral forces such as lift and drag using the velocity and pressure data field obtained. [11] These forces were then used to find its corresponding coefficients using Eq. 20 and 21. The results for the coefficients of lift and drag in both opened and cupped wings are highlighted in *Table 1* shown below.

Table 1: Comparison of lift and drag coefficients for Opened and Cupped wing configurations.

Flow Parameter	Opened Wing	Cupped wing
Lift Coefficient, $C_L$	0.0851	0.1119
Drag Coefficient, $C_D$	0.0892	0.0725

It can be concluded from B. Ponitz et al., that cupped wings were used to increase lift and decrease drag under the same flow conditions. [11] Although the total surface area of the cupped wing is larger, the overall body drag is reduced. [11] This is due to the reason that the flow acceleration close to the body through the gaps between the wings and the main body occurred during this configuration. [11] In return, this led to a shift of flow separation towards the trailing edge of the body, which reduced the form drag. [11] All in all, the numerical simulations successfully provided insights on the aerodynamics of the open and cupped shape models but lacked to consider the effects of feathers as the bird body model was considered to have a smooth surface.

Finally, during the M-shape configuration that is adopted towards the end of dive, the stoop was characterized by vortex dominated flow. [6] The experiments and simulations revealed that vortices rose from the frontal and dorsal regions due to strong spanwise flow promoted by the forward sweep, as shown in Fig. 8. [6] These vortices enabled flow reattachment towards the tail. Moreover, the strong wing and tail vortices provided extra aerodynamic forces through vortex induced lift, also shown in Fig 9. [6] The study of vortices emanating during M-shape configuration showed how the falcon was able to stabilize and exhibit superior manoeuvrability.

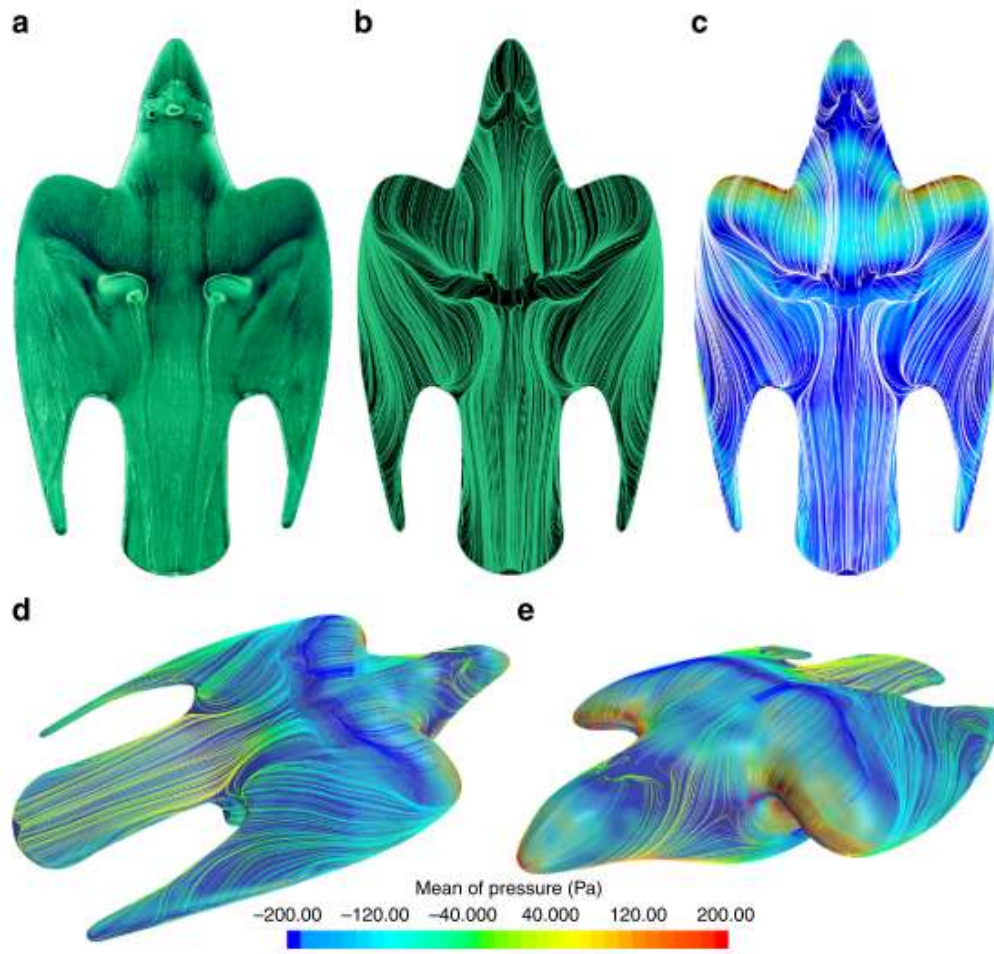


Figure 9: Surface streamline pattern showing flow topology over falcon [6]

### 3. KINEMATIC DIVE MODEL

This section deals with understanding kinematic intuition involved during falcon dive. From the mathematical model presented earlier, it was seen that during the non-equilibrium phase, the models considered either of two scenarios, i.e., constant flight path angle with varying speed (rectilinear accelerated motion) or constant speed with varying flight path angle. Moreover, maximum lift considered was limited by the component of weight acting opposite to the direction of lift produced. Nevertheless, from Ponitz et al. it can be observed that falcon was able to vary both, that is, change the glide path angle and speed at the same time. [2]

In an attempt to provide intuition behind the falcon dive kinematics, it is important that a coordinate system be established. Referring to Fig. 10, the drop in altitude is considered positive downwards on the y-axis, and motion towards right on the x-axis is considered positive. The flight path angle is considered positive counter-clockwise, such that  $\theta$  is zero initially with respect to the y-axis and perpendicular to the x-axis shown. While recovering from the dive, the falcon ends up perpendicular to the y-axis and is parallel to x-axis. Therefore, the rate of change of the flight path angle  $\dot{\theta}$  is positive in the counter-clockwise direction.

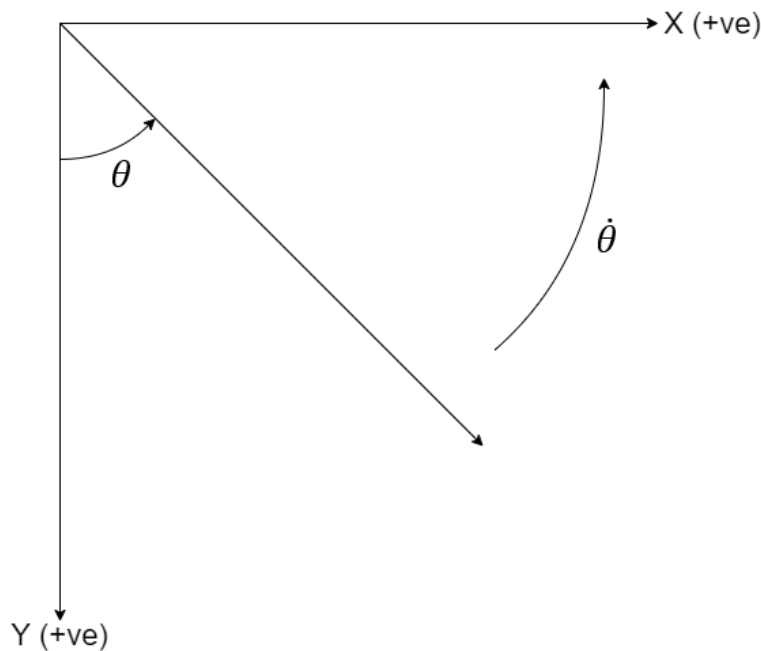


Figure 10: Falcon dive coordinate system

In Fig. 11, consider that the falcon starts from point A above the ground; this is also point of origin. The falconer is considered to be standing at point E on the ground. During the initial part of the dive, when the falcon travels from point A to B, the dive can be considered as a straight dive with the arc of the circle almost equal to a straight line. Further, in its dive path from B to C (Phase 1), the falcon accelerates tangentially with the aim of attaining maximum velocity. Simultaneously the falcon is also performing steady pull out, therefore causing acceleration in both the tangential and normal directions. It does so by minimizing drag and by using acceleration due to gravity at its advantage. Between points C-D (phase 2), the falcon travels at a constant speed phase, and it

changes its glide path angle too. Finally, when the falcon travels from points D-E (phase 3), it decelerates and makes itself parallel to the horizontal axis.

In the above model, the falcon can be imagined as ball of mass,  $m$ , attached to a string with tension  $T$ , originating from point  $O$ . Throughout the motion from points A-E, the ball increases its reference area while the tension in the string increases, and perpetually pulls it towards point  $O$ . This model can be treated as a complex spiral motion with variable acceleration.

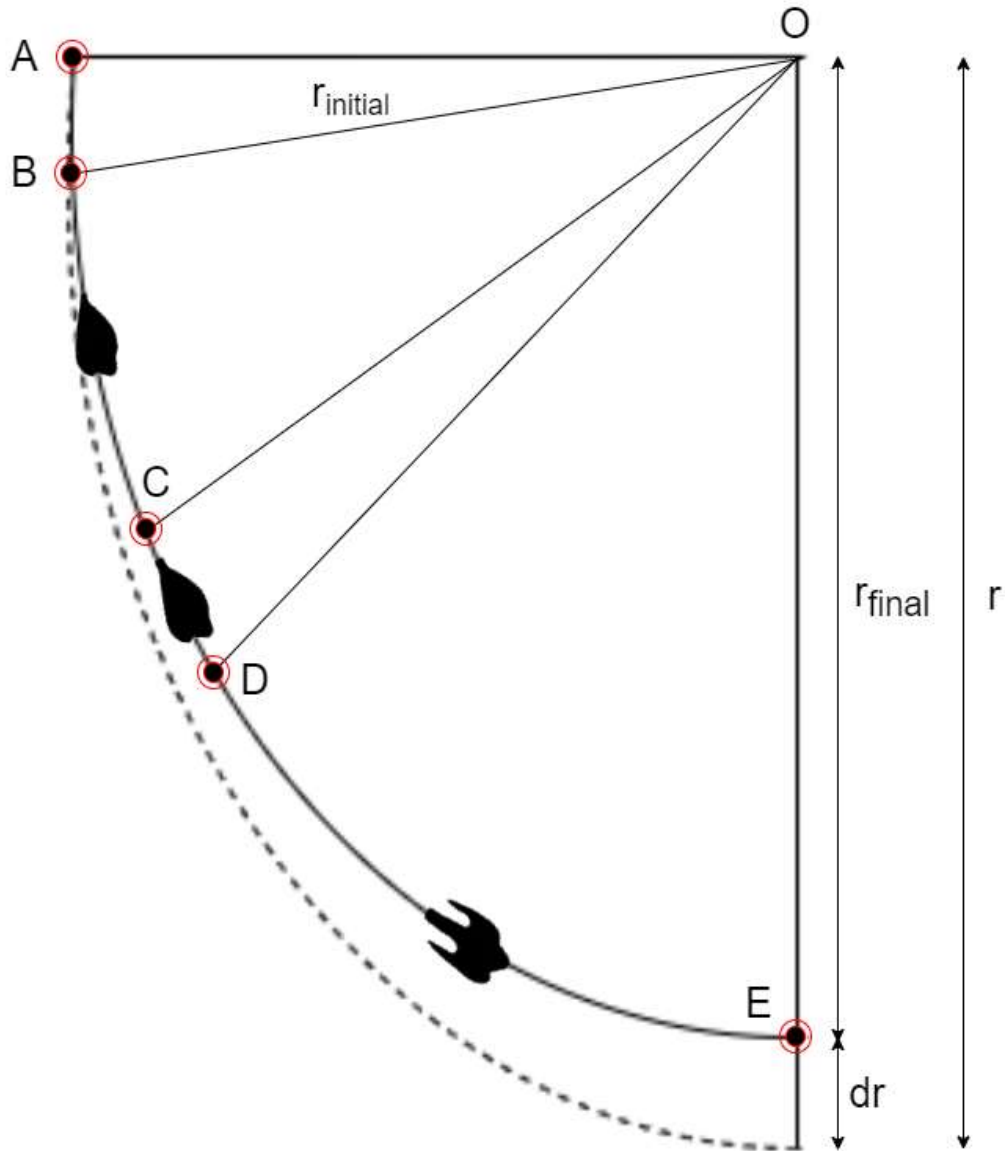


Figure 11: Phases of Falcon Dive

#### 4. ATTEMPTED MODEL AND DISCUSSION

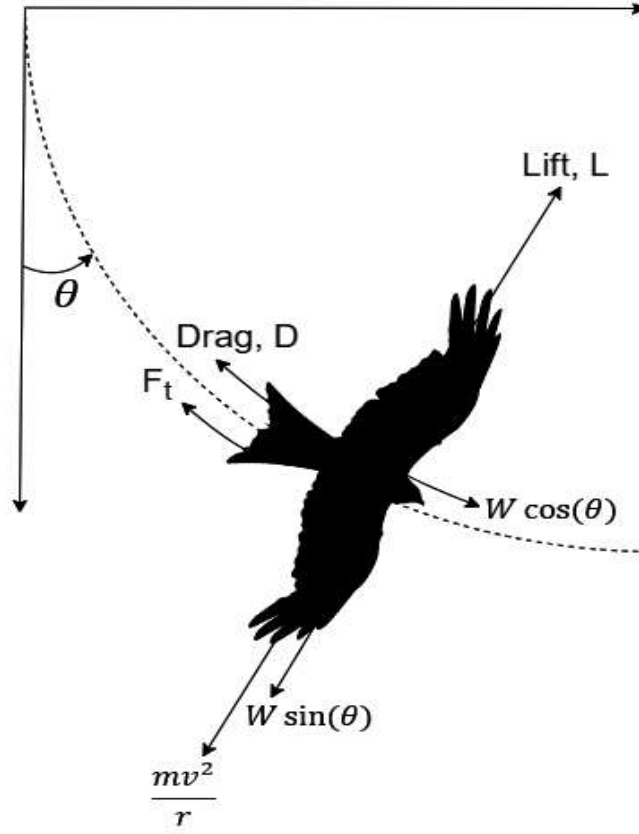


Figure 12: Forces acting on falcon when in non-equilibrium phase.

Based on the kinematic intuition of dive, the instantaneous lift of the falcon can be considered as the sum of the forces that overcome the centrifugal and normal components of weight as shown in Fig. 12 and depicted by Eq. 25. The values for initial velocity were eyeballed as 15 m/s with an acceleration of 5.5 m/s<sup>2</sup> from Ponitz et al. The normal acceleration  $a_n$  was found using Eq. 26.

$$L = W \sin \theta + \frac{mv^2}{r} \quad (25)$$

$$a_n = \frac{v^2}{r} = v \dot{\theta} \quad (26)$$

Likewise, the tangential force  $F_t$  (represents force due to inertia, resulting motion is in  $W \cos \theta$  direction, in Fig. 12) and acceleration with which the falcon glides can be written as shown in Eq. 27. The tangential acceleration was found by dividing Eq. 27 by mass as shown in Eq. 28.

$$F_t = W \cos \theta - Drag \quad (27)$$

$$a_t = g \cos \theta - \frac{Drag}{m} \quad (28)$$

The instantaneous lift from Eq. 25 was then used to obtain to  $C_L$ , which was used to obtain corresponding  $C_D$  from the drag polar provided in Ponitz et al and drag using Eq. 4. [2] Using

normal and tangential accelerations, the overall acceleration was found using Eq. 29. The total acceleration was then used to obtain next velocity using Eq. 30, assuming that for very small-time intervals, the motion was rectilinear motion.

$$a = \sqrt{a_n^2 + a_t^2} \quad (29)$$

$$v_{final} = v_{initial} + a * t \quad (30)$$

Once the velocity was obtained using Eq. 30, the procedure was repeated with a new velocity for the remaining time. However, the procedure shown above did not yield desired results. This may be due to few reasons, one of them being that the drag polar used was developed specifically for teardrop shape (or initial open cupped wing shape) configuration for equilibrium conditions only. Moreover, the research development so far lacked to develop a relation between the deviation of drag polar with respect to Reynolds number changes. Secondly, the model did not account for maximum acceptable torque that the wing can tolerate in phase 3 with M-shape configuration. Lastly, the equilibrium phase lasts for a very limited time interval; using aerodynamic properties specific to this point does not convey enough information about remaining time. However, it is evident from literature review that there is not one particular method that exists in its entirety that can be implemented to develop an aerodynamic solver to predict the falcon's dive.

## 5. CONCLUSION

As evident from the literature review presented, multiple aerodynamics methods have been carried out to study the falcon flight dive. The need to perform these methods was due to the fact that there were unanswered questions after each method. Moreover, this implies that not one specific method was enough to fully understand and predict the aerodynamics of falcon flight and to predict the maximum speed possible. Despite the work carried out so far, questions pertaining to role of feathers and their orientation during dive still remains uncharted. Beyond that, one such promising future research consideration will be studying the formation of boundary layer over feathers at low Reynolds number. Furthermore, all the methods so far consider constant reference areas throughout a phase for drag and lift calculation and failed to account for a slow increment throughout the phase, it is necessary that future models take this consideration. Understanding flow acceleration during cupped and open cupped wing configuration in greater detail might be useful in designing aerodynamic structures in automobile industry.

## 6. REFERENCES

1. "Peregrine Falcon," *National Wildlife Federation*. [Online]. Available: <https://www.nwf.org/Educational-Resources/Wildlife-Guide/Birds/Peregrine-Falcon>. [Accessed: 05-Apr-2021].
2. B. Ponitz, A. Schmitz, D. Fischer, H. Bleckmann, and C. Brücker, "Diving-Flight Aerodynamics of a Peregrine Falcon (*Falco peregrinus*)," *PLOS ONE*. [Online]. Available: <https://journals.plos.org/plosone/article?id=10.1371/journal.pone.0086506#:~:text=During%20a%20dive%20peregrines%20can,body%20shape%20and%20wing%20contour>. [Accessed: 05-Apr-2021].
3. V. A. Tucker, "Gliding flight: speed and acceleration of ideal falcons during diving and pull out.," *Journal of Experimental Biology*, 01-Feb-1998. [Online]. Available: <https://journals.biologists.com/jeb/article/201/3/403/7824/Gliding-flight-speed-and-acceleration-of-ideal>. [Accessed: 16-Apr-2021].
4. Selim, Omar et al. "The Peregrine Falcon's Dive: On the Pull-Out Maneuver and Flight Control Through Wing-Morphing." *arXiv: Fluid Dynamics* (2020): n. pag.
5. Lagemann, C., Gowree, E. R., Jagadeesh, C., Talboys, E., & Brücker, C. (2018). Experimental and numerical analysis of the aerodynamics of peregrine falcons during stoop flight. Deutsche Gesellschaft für Luft-und Raumfahrt-Lilienthal-Oberth eV.
6. Gowree, E., Jagadeesh, C., Talboys, E., Lagemann, C., & Brücker, C. (2018, April 05). Vortices enable the complex aerobatics of peregrine falcons. Retrieved April 06, 2021, from <https://www.nature.com/articles/s42003-018-0029-3#citeas>
7. V. A. Tucker, "Gliding birds: The effect of variable wing span," 01-Nov-1987. [Online]. Available: <https://journals.biologists.com/jeb/article/133/1/33/5413/Gliding-Birds-The-Effect-of-Variable-Wing-Span>. [Accessed: 16-Apr-2021].
8. D. L. Ragozin, "Error bounds for derivative estimates based on spline smoothing of exact or noisy data," *Journal of Approximation Theory*, 07-Sep-2004. [Online]. Available: <https://www.sciencedirect.com/science/article/pii/0021904583900424>. [Accessed: 16-Apr-2021].
9. V. A. Tucker and G. C. Parrott, "Aerodynamics of Gliding Flight in a Falcon and Other Birds," *Journal of Experimental Biology*, 01-Apr-1970. [Online]. Available: <https://journals.biologists.com/jeb/article/52/2/345/21503/Aerodynamics-of-Gliding-Flight-in-a-Falcon-and>. [Accessed: 16-Apr-2021].
10. Polhamus, E. C., "Predictions of Vortex-Lift Characteristics by Leading-Edge Suction Analogy," *Journal of Aircraft*, Vol. 8, No. 4, 1971, pp. 193–199.
11. Ponitz, B., Triep, M. & Brücker, C. Aerodynamics of the cupped wings during peregrine falcon's diving flight. *Open J. Fluid Dyn.* 4, 363–372 (2014)

## APPENDIX

Developing Flight Path Angle Equation.....	18
Developing Drag Polar Equation.....	18
Plotting Graphs .....	18

```
clc;  
clear;
```

### Developing Flight Path Angle Equation

```
t = 0:0.05:2.3;      % Used to plot Flight angle Data  
g_val = [70 69 68 67 66 65 64.7 64.5 63 62 59.5 57 56.5...  
         56 55.5 55.3 54 53.7 53 52.7 52.5 52 50.75 50 49.50 ...  
         48 47.5 46.25 45 43.75 42.5 41.25 39.75 38 36.75 32.50...  
         30.25 27.0 24.25 23 22 17.5 14 11.25 9.25 5 0];  
  
i =1;  
Gamma_val(i) = 20;  
  
for i = 1:1:46  
    Gamma_val(i+1) = Gamma_val(i) + (g_val(i) - g_val(i+1));  
end  
  
Gamma_curve = polyfit(t,Gamma_val,3);  
  
syms t  
Gamma_eq = vpa(Gamma_curve(1)*t.^3 + Gamma_curve(2)*t^2 + Gamma_curve(3)*t+...  
              Gamma_curve(4),5);
```

### Developing Drag Polar Equation

```
CD_pol = [0.11 0.09 0.08 0.07 0.07 0.07 0.07 0.07 0.07 0.08 0.08 0.09 0.09 0.0870...  
         0.1 0.12 0.12 0.13 0.13 0.14 0.14 0.17 0.19 0.22 0.24 0.27 0.31 0.35 0.39...  
         0.435 0.47 0.51];  
CL_pol = [-0.15 -0.12 -0.09 -0.06 -0.03 -0.01 0.01 0.035 0.045 0.05 ...  
         0.07 0.09 0.12 0.14 0.18 0.22 0.23 0.26 0.27 0.29 0.33 0.36 0.4 0.43 0.47 ...  
         0.5 0.53 0.55 0.57 0.58 0.585];  
DP_curve = polyfit(CL_pol,CD_pol,2);  
  
syms p  
DP_eq_1 = vpa(DP_curve(1)*p.^2 + DP_curve(2)*p + DP_curve(3),4);
```

### Plotting Graphs

```
t = 0:0.05:2.3;      % Used to plot Flight angle Data  
figure(1)  
plot(t,Gamma_val,'-+r','Linewidth',1)  
xlabel('Time (s)');  
ylabel('Flight Path angle  $\gamma$ ');
```

```
title('Flight Path Angle vs Time');
```

```
figure(2)
```

```
plot(CD_po1,CL_po1,'k','Linewidth',1)
```

```
xlabel('Coefficient of Drag-Cd');
```

```
ylabel('Coefficient of Lift-Cl');
```

```
title('Flight Path Angle vs Time');
```

